Lifetimes of well characterized hot nuclei via small-angle particle-particle correlations: ^{40}Ar + Ag (E/A = 7.8 and 17 MeV)

A. Elmaani,* John M. Alexander, N. N. Ajitanand, and Roy A. Lacey
Department of Chemistry, State University of New York at Stony Brook, Stony Brook, New York 11794

S. Kox, E. Liatard, F. Merchez, T. Motobayashi,† B. Noren, C. Perrin, D. Rebreyend, and Tsan Ung Chan
Institut des Sciences Nucléaires de Grenoble,
IN2P3-Centre National de la Recherche Scientifique/Université Joseph Fourier,
53 Avenue des Martyrs, F 38026, Grenoble CEDEX, France

G. Auger and S. Groult
Grand Accelerateur National d'Ions Lourds, Boite Postale 5027, 14021 Caen CEDEX, France
(Received 11 May 1993)

Particle-particle correlations are studied for large- and small-angle separations for the reactions 312 and 680 MeV ^{40}Ar + ^{nat}Ag. The spectral shapes and angular anisotropies allow a characterization of the effective temperatures and spin zones of the hot nuclear emission sources. Small-angle correlations are compared to reaction simulations that employ various parametrizations for the emission time scales. We conclude that the initial lifetime scale for ^{1,2,3}H particle evaporation is of the order of 10^{-22} s. These times are so short as to suggest a breakdown of the concept of "sequential evaporation," for which a new ansatz is explored.

PACS number(s): 21.10.Tg, 25.70.Pq

I. INTRODUCTION

An important goal of heavy ion reaction studies is to explore the characteristics of hot nuclei (e.g., [1,2]) and how they change with excitation energy. For excitations of say $\approx$ 1 MeV/ emitter nucleon, the compound nucleus concept is well established, although there are many details that need clarification. Now the emphasis is on the evolution of hot nuclei as their excitation energy is increased. In recent years particle-particle correlation measurements have been used much more extensively in studies of such hot nuclei and in particular have been used to probe their lifetime scales (e.g., [3–9]). Such studies are particularly useful if the emission source can be characterized in terms of its initial mass, charge, excitation energy, and spin zone (e.g., [10]). In 1991 we published a paper on a study of source characterization along with lifetime characterization for the systems 7 and 17A MeV ^{40}Ar + Ag [9]. In this paper we elaborate on more of these measurements and more aspects of their analyses.

The time scale that describes the fast nuclear reaction processes at impact is very short, on the order of $\approx 10^{-22}$ s; it is defined by the transit time of a nucleon across the nucleus. Fusion-evaporation reactions are expected to require a time scale of many such nuclear periods ($> 10^{-22}$ s) for successive particle decay; the active spacial extent or reaction volume for such processes covers the whole composite system [11]. These composite nuclei deexcite via evaporation of light charged particles and neutrons with essentially Maxwellian energy distributions. After a complex decay chain, the cold or stable nuclei that remain are the evaporation residues (ER's) or fission fragments (FF) [12].

One way to identify such fusion reactions, at incident energies that are not far above the entrance-channel barrier (5–10A MeV), is the measurement of the angular distributions of evaporated light charged particles (LCP) (^{1,2,3}H , ^{4}He) and neutrons. These distributions are symmetric about 90° in the emitter frame if the emitter is at thermal equilibrium. They are often nearly isotropic, providing a good signature for the existence of thermalized emitters [13]. The relative extent of energy deposition in these reactions can be estimated via the number or multiplicity of LCP's and neutrons emitted (e.g., [14–16]).

In a recent experiment, such multiplicities for light charged particles (^{1,2,3}H and ^{3,4,6}He) were measured [16] with large geometrical acceptance ($\approx$ 85%), for ^{40}Ar on ^{nat}Ag at four bombarding energies [280 (7), 680 (17), 1080 (27) and 1350 (34) MeV (A MeV)]. A sample result from these experimental observations is shown in Fig. 1, where the multiplicity distributions for the observed H and He isotopes are shown as a function of the incident ^{40}Ar beam energy. The first two incident energies (7 and 17A MeV) are of particular interest to us in conjunction with this study. (A similar study for the higher energies is now in progress.) The average multiplicity (indicated by the arrow) shows a strong increase from 7 to 17A MeV, indicating a concomitant increase in the energy

*Present address: University of Washington, Nuclear Physics Lab GL-10, Seattle, WA 98195.
†Permanent address: Department of Physics, Rikyo University, 3 Nishi-Ikebakuro, Toshima, Tokyo 171, Japan.

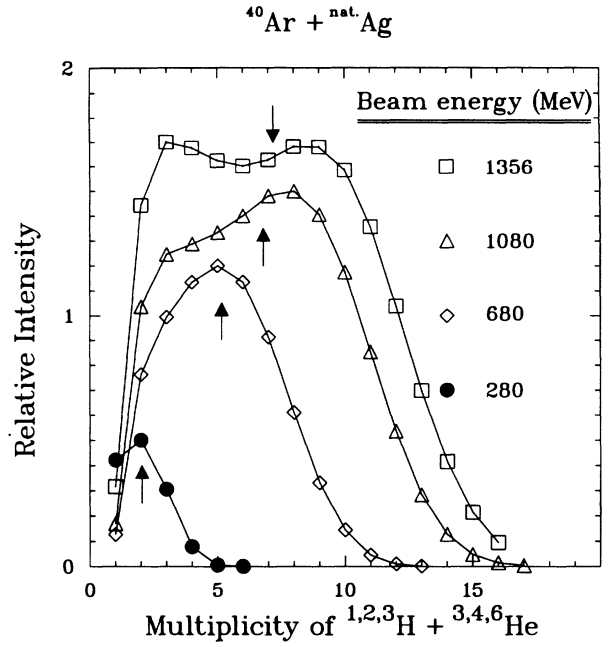

FIG. 1. Light charged particle multiplicity distributions for the reaction ^{40}Ar + ^{nat}Ag at four incident beam energies. The arrows indicate the average multiplicity for a given energy (after [16]).

deposited. For the higher energies (27 and 34A MeV) the curves become increasingly skewed to lower multiplicity values. This can be attributed to an increasing yield of peripheral reactions with low fractional energy deposition.

As the bombarding energy is increased, the cross sections for fusionlike reactions are found to saturate [12] and the average fractional energy deposition is also found to decrease (e.g., [17,18]). It appears that the incomplete fusion mechanism has become the primary route to the production of the very hot nuclei [15,19,20].

The composite nucleus $^{147-9}$Tb* formed with temperatures of $\approx$ 3 MeV has been studied in great detail [10]. Cross sections, angular distributions, and energy spectra for light charged particles (especially ^{1}H and ^{4}He) have been measured and compared with great care to calculated spectra produced by statistical modeling (see, for example, [21]). Coincidence measurements were made to evaluate the extent of thermalization in these reactions, as well as the momentum transfer to the emitter. Invariant cross section maps for particle-particle coincidences, indicate that the emitter velocity is consistent with the *center-of-mass* velocity, i.e., a signature for essentially complete momentum transfer to the emitter at these energies ($\approx$ 6 to 8A MeV). In addition to these observations, the measured energy spectra were very relaxed. This confirmed that complete thermalization occurs for this compound nucleus (CN) with excitation energies up to $\approx$ 200 MeV [22].

For incident energies even up to tens of MeV per nucleon, a metastable CN may still be formed due to the continuing power of the attractive mean nuclear field (see, for example, [23,24]). If its lifetime is longer than the time needed for complete energy mixing, then thermalization of the CN can be said to have been achieved. The evaluation of the mean lifetime τ of the CN is, therefore, very valuable for our understanding of the dynamics of equilibration processes. In addition, the dependence of the mean lifetime on excitation energy can be of even greater value in the search for limiting conditions for an equilibrated CN [7–11].

To pursue these goals, we have chosen to study the same reaction system, ^{40}Ar on ^{nat}Ag at 312 and 680 MeV. First we test for consistency with the previous study [10], using large-angle particle-particle correlations. Then we use the small-angle correlations to estimate the lifetime and hence to test for the extent of equilibration of $^{147-9}$Tb*. We also use a beam energy of 680 MeV ^{40}Ar to try to produce a much more highly excited system and test for its degree of thermalization. A key point here is the selection of the particular central collisions most likely to lead to composite nuclei. This source selection is an important prerequisite to an informative utilization of lifetime measurements; otherwise a mixing of reaction mechanisms can lead to misleading interpretations.

From the previous study [10] it has been concluded that two particles detected in coincidence at side angles ($\theta_{lab} > 60°$) are quite selective for those reactions with high-energy deposition (central collisions). To confirm this, more experimental evidence can be found in Refs. [15,16,20], where a 4π detector [25] was used. In that work the multiplicity distribution of light charged particles has been used to distinguish between central and peripheral collisions. An example of that separation is shown in Fig. 2, where the multiplicity associated with two particles detected at $\theta_{lab} \approx 67°$ indicates that central collisions of maximum violence have indeed been selected. Low velocity heavy fragments (i.e., ER's) are often asso-

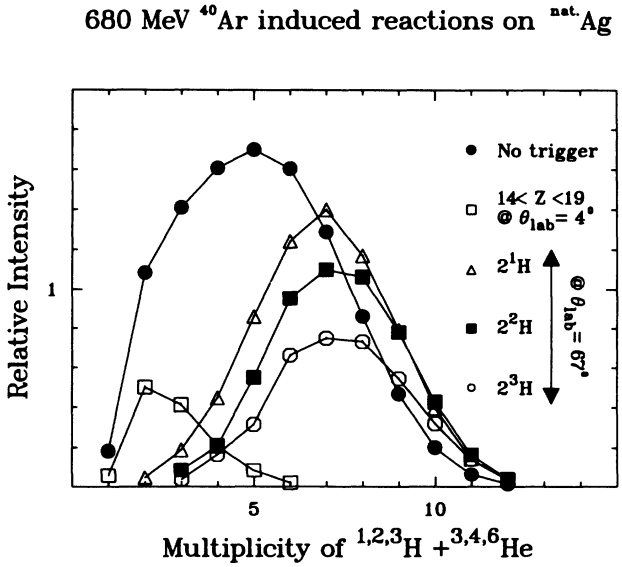

FIG. 2. Gated light charged particle, (^{1,2,3}H and ^{3,4,6}He), multiplicity distributions measured for 17A MeV ^{40}Ar induced reactions on ^{nat}Ag. Trigger conditions are indicated.

ciated with such collisions [12,18,19,24]. On the other hand when a high-velocity heavy fragment is detected in the forward direction, it is more likely to be associated with a projectile remnant from a peripheral collision thus leading to fewer emitted particles.

In the experimental work reported here, we emphasize detection of particle pairs at a large angle ($\approx 67°$). In this way we select the central-collision reaction class, but we also use the detailed results of these particle-particle correlations to study the decay properties of the hot nuclei formed. For reactions at much higher energies these particle correlations give a probe of the size of the collision zone [3,26]. In this energy domain they give a means for testing the time scales of the reaction [6–9,11,27].

II. CHARACTERISTICS OF ^{147,149}Tb* COMPOSITE SYSTEMS

A theme of this work is the selection and characterization of a set of hot nuclei in conjunction with a study of their lifetimes by means of particle-particle correlations. For both 7 and 17A MeV ^{40}Ar + Ag it has been shown that the more central collisions lead to fusion, and that the detection of a pair of charged particles is sufficient to select these fusing collisions. From the systematics of linear momentum transfer one can estimate that for 17A MeV ^{40}Ar the initial composite nucleus is excited to ≈ 430 MeV or to a temperature of ≈ 5 MeV. We use the measured energy spectra and large-angle correlations

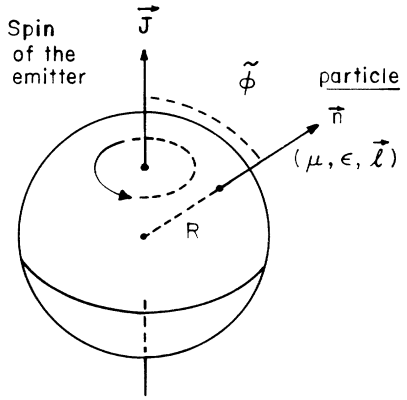

$$d\Gamma_{E,J}(\vec{n}) \propto \exp(\beta_2 \sin^2\tilde{\phi})$$

$$\langle \epsilon \rangle_{\tilde{\phi}} = B + T + T\left[\frac{\mathcal{J}_d}{\mathcal{J}_d + \mu R^2}\right](1 + \beta_2 \sin^2\tilde{\phi})$$

$$\beta_2 = \frac{\hbar^2 (J+1/2)^2}{2\mathcal{J}_d T}\left[\frac{\mu R^2}{\mathcal{J}_d + \mu R^2}\right]$$

FIG. 3. Schematic diagram for emission of a particle (reduced mass μ, channel energy ϵ, orbital angular momentum l) in the direction **n** at angle ϕ to the spin **J** of a spherical emitter of excitation energy E^*. The emission radius is R, emission barrier is B, and daughter moment of inertia is $\mathcal{J}_d$. Emission width is $d\Gamma$ and anisotropy parameter is β_2 after [9].

to rexamine this estimate and to determine additional properties of the emission source. For this task we follow the procedure of Refs. [9,10] in using reaction simulation calculations based on the equilibrium statistical model.

To get a simple feeling for the statistical theory, we first recall an intuitive description of the classical picture from the schematic diagram in Fig. 3. Particle emission from a spinning nucleus can be pictured as emission of a charged, but sticky granule from the surface of a charged rotating sphere. Emission probability $d\Gamma_{E,J}$ at a direction **n** (or angle ϕ) is axially symmetric but anisotropic; the average energy $\langle \epsilon \rangle_\phi$ also depends on ϕ. The strength of these anisotropies is determined by β_2 the ratio of the rotational energy of the granule on the emission surface to its temperature T, where μ is the reduced mass, **J** is the spin of the spherical emitter, $\mathcal{J}_d$ is the daughter moment of inertia, and R is the emission radius. Therefore, the anisotropy increases with rotational energy of the emitter and with mass and radius of the granule, but decreases with increasing temperature or moment of inertia. Of course, the average emission energy $\langle \epsilon \rangle_\phi$ increases with increasing temperature, but it decreases with radial expansion due to a concomitant decrease in the energy of the Coulomb barrier B.

III. EXPERIMENTAL WORK ON LARGE-ANGLE CORRELATIONS

Our experimental study of the emission source follows a well-established approach. In Ref. [10] inclusive and exclusive measurements were made of ^{1}H and ^{4}He from ^{nat}Ag irradiations by ^{40}Ar of 6.2 and 8.5A MeV. By using a statistical model reaction simulation, they extracted from the large-angle correlations the average excitation energy (and associated temperature), rms angular momentum, and effective emission barriers. In this work we study the same reaction system (^{40}Ar + ^{nat}Ag) at both a very similar energy 7.8A MeV, and at a much higher energy, 17A MeV.

The 16 detector array (EMRIC [28]) used in this study is shown in Fig. 4 along with the in-plane (IP) and out-of-plane (OP) trigger detectors centered at $\theta_{lab} \approx 68°$ or $\theta_{c.m.} \approx 90°$. Energy spectra were recorded in these IP, OP triggers as well as in EMRIC, also centered at $\theta_{lab} \approx 68°$. In Fig. 5 we show four pairs of energy spectra, each recorded in the EMRIC array . Those on the left (right) result from ^{4}He-^{4}He (^{1}H-^{1}H) coincidences; the solid (open) points are from the reaction with ^{40}Ar of 312 MeV (680 MeV); the circles (squares) are from IP (OP) coincidences with the single detector shown in Fig. 4 on the right of (above) the beam axis [both placed at ($\theta_{lab} \approx 68°$)]. The data in Fig. 5 give a lot of information about the reactions.

Let us begin by examining the solid points on the right for ^{1}H from 312 MeV ^{40}Ar + ^{nat}Ag. They show classic Maxwellian-like shapes for proton evaporation: a sharp rise at low energies from ≈ 4 to 8 MeV, a maximum at ≈ 9 MeV, and a straight exponential decline for energies ≥ 12 MeV. The maximum for the IP data is normalized to 6000 per MeV; bin-by-bin ratios of the IP to OP spectra are shown by triangles on the lower scale. Here these

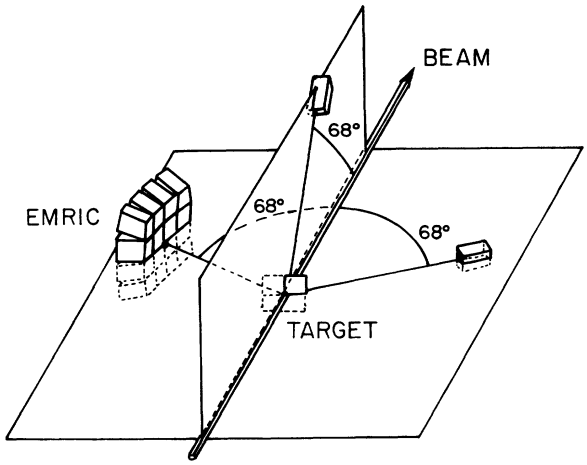

ENSEMBLE DE MESURE RAPIDE POUR L'INTERFEROMETRIE ET LES CORRELATIONS

FIG. 4. The experimental setup: EMRIC was centered at 68° with respect to the beam; two CsI detectors were placed at 68° (opposite to EMRIC) in plane and out of plane.

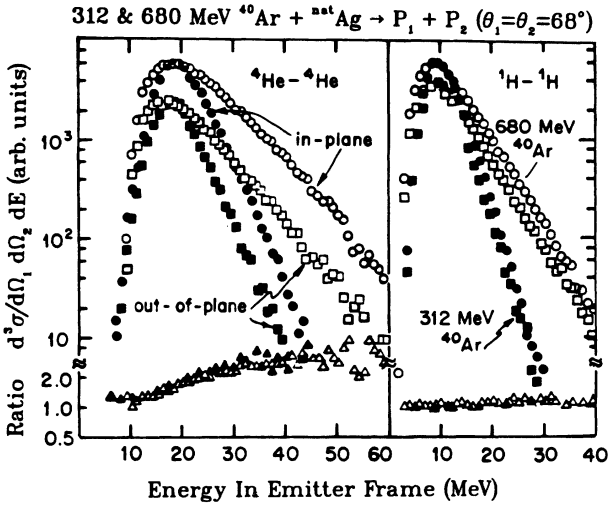

FIG. 5. Energy spectra recorded in EMRIC for ^{1}H-^{1}H and ^{4}He-^{4}He pairs; solid points for 312 MeV ^{4}Ar; open for 680 MeV; circles for in-plane (IP) coincidences; squares for out of plane (OP). Triangles show the anisotropy ratios IP/OP. Emitter frame transformations assumed 100% and 85% momentum transfer, respectively, for 312 and 680 MeV ^{40}Ar, after [9].

ratios are essentially unity for all proton energies, i.e., there is no significant anisotropy.

Let us now compare the data for protons from 312 and 680 MeV ^{40}Ar; we see the same classic evaporation shapes. The high-energy spectral slope given by

$$\frac{1}{\tilde{T}} = -d\ln\frac{\sigma(\epsilon)}{d\epsilon} \tag{3.1}$$

has changed from $\tilde{T}$ of 2.4 to 5.0 MeV, and the average proton energy has increased from 10.5 to 11.9 MeV. This rather small increase in $\langle\epsilon\rangle$ results because the spectrum has also broadened at low energies to give more particles of < 10 MeV. Finally, the angular anisotropy has increased from 0.99 to 1.09 in favor of the IP over the OP configuration. The same pattern is also exhibited by the ^{4}He-^{4}He data, but each quantity is larger than that for ^{1}H-^{1}H. Spectral slopes change from 3.6 to 6.8 MeV, and the average energies from 20.0 to 23.4 MeV.

The angular anisotropy increases with energy from almost unity for alphas of $\epsilon \leq 10$ MeV to IP/OP ≥ 2 for those alphas of $\epsilon \geq 30$ MeV. Energy integrated anisotropies for the ^{4}He-^{4}He pairs increase with beam energy from 1.82 to 1.92. Spectral slopes $\tilde{T}$, average ϵ, and anisotropy ratios are given in Table I for other pairs, ^{1}H-^{2}H, ^{2}H-^{2}H, and ^{1}H-^{4}He, as well.

TABLE I. Spectral slopes $\tilde{T}$ in MeV, average energies $\langle\epsilon\rangle_{IP}$ (MeV), and anisotropy ratios IP/OP.

	312 MeV ^{40}Ar + ^{nat}Ag			680 MeV ^{40}Ar + ^{nat}Ag			
Particles	$\tilde{T}$	$\langle\epsilon\rangle_{IP}$	IP/OP	$\tilde{T}$	$\langle\epsilon\rangle_{IP}$	IP/OP	$\tilde{T}_{680}/\tilde{T}_{312}$
Protons							
^{1}H-^{1}H	2.4	10.5	0.99	5.0	11.9	1.09	2.1
^{1}H-^{2}H	2.3	10.3	1.04	5.2	11.9	1.13	2.3
Deuterons							
^{2}H-^{1}H	2.7	13.7	1.04	6.6	15.2	1.13	2.9
^{2}H-^{2}H				6.1	15.1	1.25	
Alphas							
^{4}He-^{1}H	3.4	19.6	1.17	6.8	22.6	1.27	2.0
^{4}He-^{4}He	3.6	20.0	1.82	6.8	23.4	1.95	1.9

A. Temperature, spin zone, and radial extent

The features of the mechanical analog model, described in Fig. 3, also result from a more complete statistical model. Therefore, they allow us to make a simple qualitative interpretation of the observations given in Fig. 5. First, the spectral slopes $\tilde{T}$ increase about twofold, a reasonable increase for the expected increase in energy and spin deposition by fusion reactions of 7.8–17A MeV ^{40}Ar. However, there are rather modest increases in the average energies $\langle\epsilon\rangle$ due to an increase in the abundance of low- as well as high-energy particles. This increase in low-energy particles signifies a decrease in the average Coulomb barrier to particle emission. Finally, the slight increase in angular anisotropies indicates somewhat larger anisotropy parameters (β_2). Since the temperature has also increased, this increase in β_2 points toward a significant increase in the emitter spin.

These observations have been interpreted more quantitatively by use of the statistical-model simulation code GANES [29]; we have made fits (details discussed in [10]) to the ^{1}H and ^{4}He data in order to obtain the parametrizations of average emitter characteristics listed in Table II. As discussed above, the root-mean-square emitter spin $J_{\rm rms}$ has increased along with β_2, the anisotropy parameter. The effective temperatures have also increased, and the emission barriers have decreased due to charge loss and emitter distention. Such evidence for radial distention has been previously reported [10] for ^{40}Ar induced reactions at $\approx 8A$ MeV on $^{\rm nat}$Ag. The major point here is that the qualitative role of the effective Coulomb barriers is quite evident in the low-energy cutoffs of the spectral shapes. Hence the notion still obtains particles evaporating from a rather compact source, held together by its mean field even for spectral temperatures of ≥ 5 MeV. If the source size were to be greatly expanded, then the effective barrier would be greatly reduced (inversely with the effective radius).

In fact, all of these observations are consistent with a reasonable picture for the properties of a thermalized, but very hot and somewhat swollen compound nucleus. Furthermore, the statistical model provides a formula [11], simply from phase space considerations, to estimate the emission lifetimes of such hot compound nuclei. This formalism was derived by reference to the principle of detailed balance, for a parent emitter A that decays to a daughter nucleus B via emission of a particle p, where ρ is the level density of the state (A for the initial and B for the final) and w^*_{BA} represents the transition rate for the inverse reaction. If one sums over all the available states, one can deduce the decay rate in a simple form,

$$(\tau)^{-1} = \int\int \frac{\rho_B \; w^*_{BA}}{\rho_A} \, d\epsilon \, d\ell \; .$$

We have made such calculations [30,31] for the reactions of interest here, namely the 312 and 680 MeV ^{40}Ar on $^{\rm nat}$Ag. These calculated partial mean lifetimes for a pair of evaporated protons are plotted in Fig. 6. In this figure a main feature is in the overlap of the late decay steps of the 680 MeV reaction with the very early ones at 312 MeV. This indicates that the average delay time between the emission of two protons in the low-energy reaction should be relatively long, while the same kind of evaporative emission for the higher energy should also include pairs with much shorter delays. The results of these correlations are shown and discussed below in Sec. IV, where we present measurements and calculations relevant to the decay times for these compound nuclei. First we summarize the angle-integrated cross sections.

B. Cross sections for particle-particle coincidences

As previously stated, we have made singles and coincidence measurements using a substantial number of detectors placed at various angles. From these measurements, we were able to extract relative cross sections for many particle-particle pairs as given in Table III. In this section we explain the method of integration used, as well as their normalization to obtain absolute cross sections.

TABLE II. Statistical properties of the composite nucleus emitters.

	312 MeV ^{40}Ar + $^{\rm nat}$Ag		680 MeV ^{40}Ar + $^{\rm nat}$Ag	
	^{1}H - ^{1}H	^{4}He-^{4}He	^{1}H - ^{1}H	^{4}He-^{4}He
$J_{\rm rms}(\hbar)$	50	50	64	64
β_2	0.43	1.7	0.58	1.8
B (MeV)	6.0	13.2	4.5	11.9
$B_{\rm fus}$ (MeV)	8.49	15.9		
$\langle$FEL$\rangle$	0.33	0.33	0.4	0.25
$\langle$T$\rangle$ (MeV)	2.2	2.2	3.4	4.0

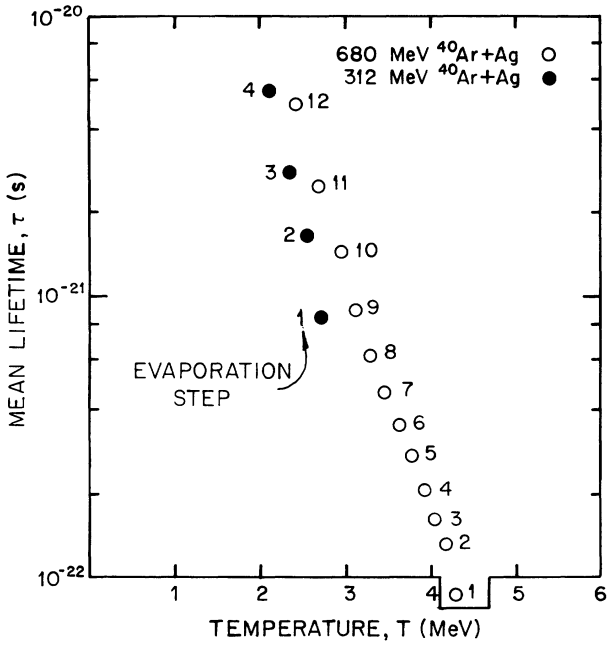

FIG. 6. Calculated mean lifetimes τ versus temperature and evaporation step for the two reactions of interest.

1. *Angle-integrated particle-particle cross sections*

For the angular integration of the experimental differential cross sections we have focused on two trigger detectors [both placed at $\approx 68°$ in plane (IP) and out of plane (OP)] and EMRIC as the sweeper. We also include those coincidences recorded in EMRIC alone. The transformations from laboratory to emitter frame were carried out on an event by event basis, for both energy and angle, and then the double integration was performed

$$\sigma_{p1p2} = \int\int \frac{d^2\sigma}{d\Omega_{p1}d\Omega_{p2}} d\Omega_{p1}d\Omega_{p2} \ ,$$

where σ_{p1p2} represents the integrated double coincidence cross section for a pair of particles $(p1, p2)$. We have carried out these integrations for all pairs of LCP's (^{1,2,3}H, ^{4}He) to obtain values of σ_{p1p2}; for each combination; appropriate anisotropy correction factors have been employed [10]. The final cross sections include only the evaporationlike particle emission.

2. *Normalization procedure*

The integration procedure described above provided only relative cross sections σ_{p1p2} because the Faraday cup was not absolute. (It was located far downstream from the target.) We then obtained absolute cross sections by normalizing to experimental values from Refs. [10] and [32]. For 312 MeV ^{40}Ar we used the measured cross section for coincident α's $\sigma_{\rm DC}^{\alpha\alpha} = 1.142 \pm 0.034$ b as the reference cross section value [10]. And for 680 MeV ^{40}Ar we used the proton-proton pairs for the absolute value [32] $\sigma_{\rm DC}^{pp} = 18.2 \pm 0.5$ b. The resulting cross sections for particle-particle pairs at both energies are listed in Table III. The experimental results are generally consistent with those from the earlier works but include many more particle types. They will be used as tests for the statistical model in a future study. We present them here for completeness.

3. *Average particle energies*

In Sec. II and [8,9], data from large-angle correlations have been used to characterize the initial excitation energies and spins of the emitting nuclei. The average energies of the light particles, listed in Tables IV and V also give an interesting impression of the emitter systems. These values for each particle do not change for different coincident partners; hence these changes do not appear to

TABLE III. Angle integrated particle-particle cross sections (σ in b), including only evaporative components.

P_1-P_2	312 MeV ^{40}Ar+$^{\rm nat}$Ag	680 MeV ^{40}Ar+$^{\rm nat}$Ag
σ^{pp}	1.660	18.20
σ^{pd}	0.186	5.903
σ^{pt}	0.058	2.730
$\sigma^{p\alpha}$	2.120	27.74
σ^{dd}	0.004	0.443
σ^{dt}		0.420
$\sigma^{d\alpha}$	0.126	5.786
σ^{tt}		0.070
$\sigma^{t\alpha}$	0.032	2.076
$\sigma^{\alpha\alpha}$	1.142	17.83

TABLE IV. Average energies $\langle\varepsilon\rangle$ for coincident particles (p, d, t, α) in the emitter frame. Measurements were made in the EMRIC array at $\approx 90°$ in the emitter frame for 312 MeV ^{40}Ar+$^{\rm nat}$Ag. We assume full momentum transfer [4].

P_1-P_2	$\langle\epsilon_p\rangle$	$\langle\epsilon_d\rangle$	$\langle\epsilon_t\rangle$	$\langle\epsilon_\alpha\rangle$
p-p	10.45			
p-d	10.28	13.68		
p-t	10.32		14.11	
p-α	10.35			19.68
d-d		13.48		
d-t		13.24	14.53	
d-α		13.63		19.61
t-t			13.50	
t-α			14.30	19.67
α-α				19.83

TABLE V. Average energies $\langle\varepsilon\rangle$ for coincident particles (p, d, t, α) in the emitter frame. Measurements were made in the EMRIC array at $\approx 90°$ in the emitter frame for 680 MeV ^{40}Ar+^{nat}Ag. We assume 85% momentum, mass, and energy transfer [30].

P_1-P_2	$\langle\epsilon_p\rangle$	$\langle\epsilon_d\rangle$	$\langle\epsilon_t\rangle$	$\langle\epsilon_\alpha\rangle$
p-p	11.93			
p-d	11.88	16.87		
p-t	11.85		17.43	
p-α	11.87			22.73
d-d		16.75		
d-t		17.10	17.45	
d-α		16.93		22.83
t-t			17.30	
t-α			17.63	22.85
α-α				23.05

make any special selections of emitter properties. In the most rough approximation the average energy is given by the (the average or) effective barrier and temperature averaged over the emitter chain

$$\langle\varepsilon\rangle \approx \langle B + 2T \rangle .$$

For each particle the values of $\langle\varepsilon\rangle$ change only modestly with incident energy from 312 to 680 MeV. This indicates that there is no massive temperature change as would be expected for particle emission before thermalization for the 680 MeV beam. The average energies for α particles are roughly twice those for protons, reflecting the larger Coulomb barrier for charge two versus charge one. The steady increase of $\langle\varepsilon\rangle$ with mass for the hydrogen isotopes partly reflects biases of the rare particles (^{3}H and ^{2}H) toward the higher temperatures of the early members of the emission chain [33]. Of course, many other properties of the emitter, e.g., angular momentum, are important as well. Nevertheless we get a sense from these average values, and the other results, that this study has indeed selected particle emission from thermalized nuclear emitters.

IV. TESTS OF THE PATTERN OF EMITTER LIFETIMES

A. Lifetime study via particle-particle correlations at small relative angles

In previous work, studies of the lifetime scale for particle emission have involved light nuclei [7,8], namely reactions of ^{16}O + ^{27}Al with incident energies from 80 to 250 MeV. In this work the objective is to extend the study of particle emission time scales to reactions of heavier nuclei at higher energies. For these reactions we focus mainly on the processes that form composite nuclei with initial excitation energies up to $\approx$ 400 MeV and initial temperatures up to $\approx$ 4.5 MeV.

We now turn to the small-angle particle-particle correlations for identical particles, i.e., p-p, d-d, and t-t, and make comparisons to reaction simulations in two ways: first the simple approximation of two-step emission with the mean lifetime as a free parameter, then the more elaborate multistep simulations with the level parameter fixed by the energy spectra and the lifetimes calculated from a statistical model formula. Both of these simulation calculations use the code MENEKA [30,31] in which the lifetimes of the emitting sources are the main drivers for the small-angle correlations [34].

B. Experimental small-angle correlations for identical particles

In this section we focus on the like particle pairs ^{1}H-^{1}H, ^{2}H-^{2}H, and ^{3}H-^{3}H. For the case of ^{1}H-^{1}H a substantial number of proton pairs has been recorded at both energies. Hence we are in a position to test for the role of excitation energy. (Unfortunately this is not the case for deuteron and triton pairs since the cross sections decrease dramatically with decreasing energy.) We initially consider the simplified approach of two-step emission to fit the experimental data. In the first step of this procedure we adjust the spectral parameters to describe the energy spectra of the coincident particles, using

$$P(\epsilon) = (\epsilon - V)^2 \times \exp -\epsilon/T , \qquad (4.1)$$

where T and V are the effective nuclear temperature and barrier, respectively. Then from the best fit to the correlation function we obtain an average emission time delay for the whole emission chain.

In a second procedure, we extend the simulation calculations to include a more elaborate description of sequential emission in the evaporation chain. This second approach is handled by a multistep simulation (option 2 in Ref. [31]) that takes into account the changes in temperature and lifetime that occur along the emission cascade [33]. In both cases three body trajectory calculations are carried out using the best fits to the energy spectra for the particle pairs, and the geometrical acceptances, etc., are applied to reproduce experimental conditions.

1. First approximation: Two-step emission

(1) Proton-proton correlations from reactions at 7.8A MeV: Figures 7 and 8 show results of the fits obtained from two-step emission calculations. First Fig. 7(a) gives the proton energy spectrum as described by the indicated spectral temperature T_p and barrier V_p given in MeV. This set of parameters does indeed give a reasonable fit to the observed spectrum in Fig. 7(a). Furthermore they also produce a very satisfying match to the observed relative momentum distribution of Fig. 7(b). The calculated correlation function shown in Fig. 8 was obtained using a mean lifetime $\tau_{pp} = 1 \times 10^{-20}$ s. For such a long mean lifetime the correlation function does not deviate much from unity, since the emission time delays between two successive protons is large enough for the first to almost

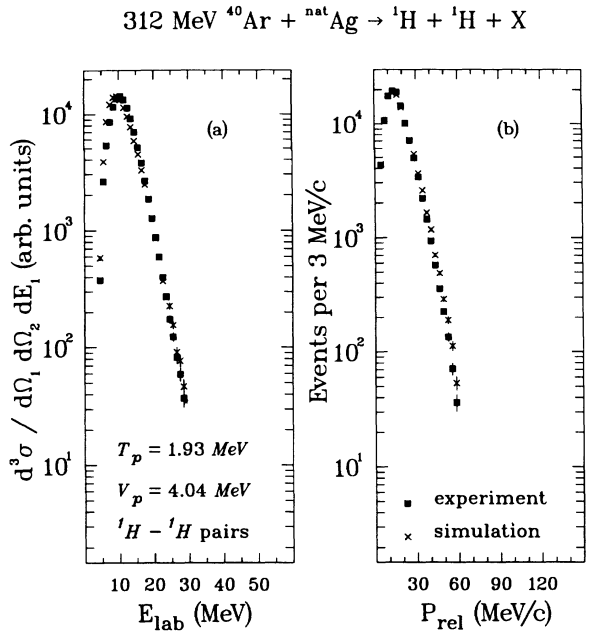

FIG. 7. Fits of the energy spectrum (a) and the resulting relative momentum spectrum (b) for ^{1}H-^{1}H particle pairs (7.8A MeV ^{40}Ar + ^{nat}Ag). The detector thresholds and resolution were 4.5 and 0.5 MeV, respectively.

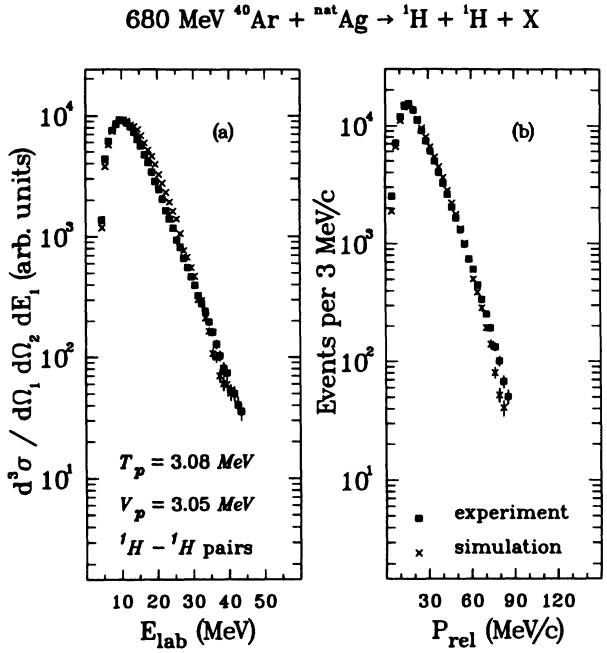

FIG. 9. Fits of energy spectrum (a) and the resulting relative momentum spectrum (b) for ^{1}H-^{1}H particle pairs (17A MeV ^{40}Ar + ^{nat}Ag). The detector thresholds and resolution were 4.5 and 0.5 MeV, respectively.

escape from the force field of the second. Indeed both experimental and calculated correlation functions are almost flat over the whole range of P_{rel}. This result gives a strong indication for adequate time to achieve complete thermalization of the ^{147,149}Tb* compound nucleus.

(2) Proton-proton correlations from reactions at 17A MeV: Using the same framework, we now turn to the p-p pairs evaporated from more excited nuclei, formed in the 17A MeV reactions. Again we begin the analysis by a fit to the proton energy spectrum measured in coincidence using the set of parameters that are indicated in Fig. 9(a). The calculated relative momentum distribution also fits the experimental distribution as shown in Fig. 9(b). Finally experimental and calculated correlation functions are compared after adjustments are made in the mean lifetime τ_{pp}. In Fig. 10 we show the result of the comparison for an average emission time delay (τ_{pp}) of 5 x 10^{-21} s. This best fit value of $\tau_{pp} \approx 5$ x 10^{-21} s was obtained after many such comparisons, in which the value of τ_{pp} was varied from 10^{-22} to 10^{-20} s.

(3) Small-angle correlations for ^{2}H-^{2}H and ^{3}H-^{3}H : As previously stated, the double coincidence cross sections for deuteron and triton pairs are very small compared to that for protons. For the 17A MeV reactions we obtain $\sigma_{DC}^{pp} = 18.2 \pm 0.5$ b, $\sigma_{DC}^{dd} = 0.443 \pm 0.012$ b, and $\sigma_{DC}^{tt} = 0.070 \pm 0.002$ b. Nevertheless we have constructed correlation functions for both d-d and t-t pairs. We follow the same approach as before to fit the energy spectra with spectral parameters for ^{2}H-^{2}H pairs and ^{3}H-^{3}H pairs. For both the deuterons and tritons, the fits to the correlation functions are again achieved

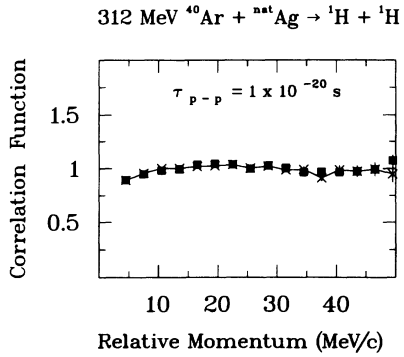

FIG. 8. Experimental correlation functions (squares) for ^{1}H-^{1}H pairs from the reaction 7.8A MeV ^{40}Ar + ^{nat}Ag. The points for the calculated correlation function are shown by crosses and joined by a line to guide the eye.

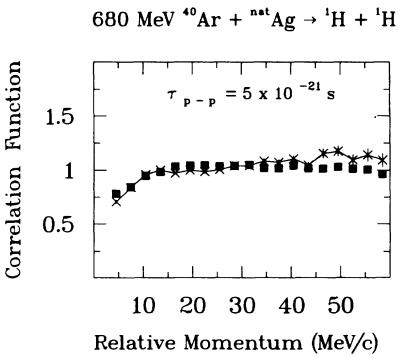

FIG. 10. Experimental correlation function (squares) for ^{1}H-^{1}H pairs from the reaction of 17A MeV ^{40}Ar + ^{nat}Ag. The points for the calculated correlation function are shown by crosses and joined by a line to guide the eye.

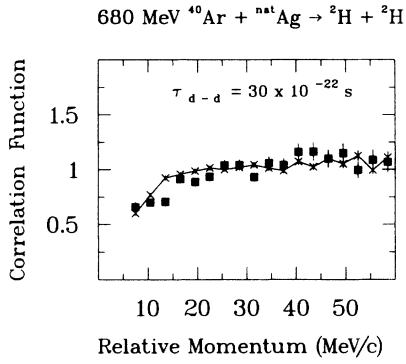

FIG. 11. Experimental correlation function (squares) for ^{2}H-^{2}H pairs from the reaction of 17*A* MeV ^{40}Ar + ^{nat}Ag. The points for the calculated correlation function are shown by crosses and joined by a line to guide the eye.

by variation of the mean lifetimes as shown for ^{2}H-^{2}H in Fig. 11 and for ^{3}H-^{3}H in Fig. 12. Even with more limited statistics it is clear that the anticorrelations for small $P_{\rm rel}$ are stronger for *t-t* than for *d-d* than for *p-p*. This trend is indicated by the mean lifetimes that give the best fits for $\tau_{tt} = 20 \times 10^{-22}$ s, $\tau_{dd} = 30 \times 10^{-22}$ s, and $\tau_{pp} = 50 \times 10^{-22}$ s. We estimate that relative uncertainties are $\approx$ 15% and absolute uncertainties are $\approx$ 30%. (See [31].) This trend of shorter mean lifetime for *t-t* compared to *d-d* compared to *p-p* is consistent with the expected biasing for the emission of unfavored particles (deuterons and tritons) toward the early emission steps in the chain [33].

2. *Second approximation: multistep emission*

In a second approach for the reaction model calculations, we use a more detailed description of the evaporation chain to compare with experimental data. The calculation allows for a series of emission steps from emitters of successively lower temperatures and longer lifetimes. The first calculations of this type were described in [7] for comparisons to data for ^{16}O+^{27}Al reactions. Here we use option 2 in MENEKA [31] in conjunction with the (Hauser-Feshbach) statistical-model code MODGAN [31,33]. Our purpose (as in [7]) is to see if the equilibrium statisical model can give a reasonable first approximation for the reaction time scales as reflected in the correlation functions.

In this approach we first choose a value for the level density parameter *a* that gives the best overall description of the energy spectra for the particle, in this case $a = A/8$. The effective barrier parameters are simply taken from the spectral fits as shown above. Since these parameters have already been fixed by consideration of the energy spectra, the calculated correlation functions become a direct test of the lifetime predictions. The only additional inputs needed are the branching ratios for neutron and proton emission at each step in the evaporation chain. This was supplied by an ancillary model calculation in which we used the code MODGAN [33]. With these input quantities MENEKA [31] carries out the multistep emission simulation taking account of stepwise emitter cooling and lifetime growth in an average way.

We begin these multistep calculations and comparisons for the case of ^{1}H-^{1}H pairs produced at 7.8*A* MeV. In Fig. 13 the information relative to this comparison is shown

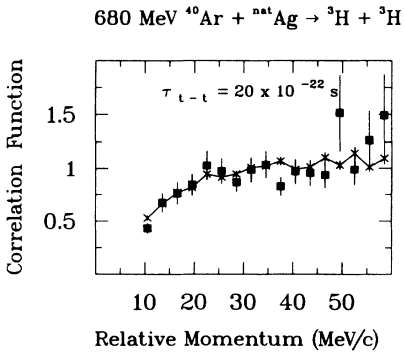

FIG. 12. Experimental correlation function (squares) for ^{3}H-^{3}He pairs from the reaction of 17*A* MeV ^{40}Ar + ^{nat}Ag. The points for the calculated correlation function are shown by crosses and joined by a line to guide the eye.

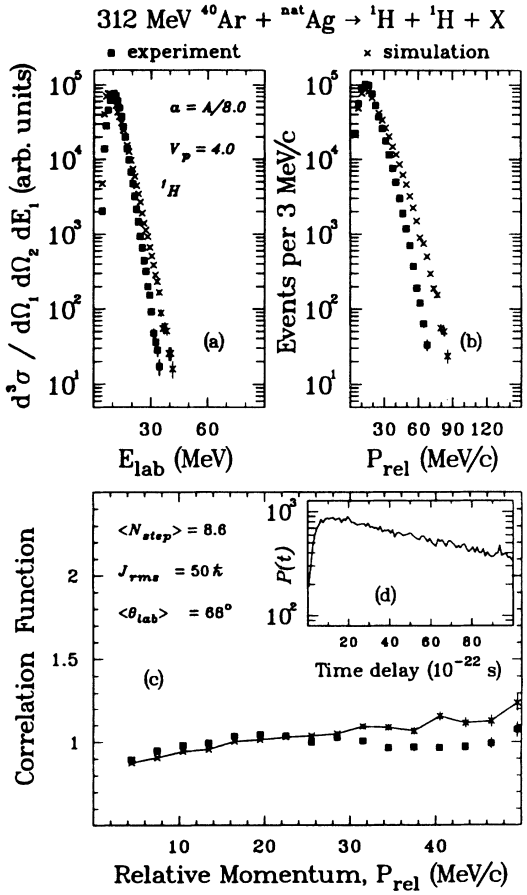

FIG. 13. Experimental and calculated (a) energy spectra, (b) relative momentum, (c) correlation functions, and (d) time delay distribution for ^{1}H-^{1}H pairs at 7.8*A* MeV ^{40}Ar + ^{nat}Ag.

in the four panels. Figure 13(a) shows the experimental data (squares) and calculated points (crosses) for the proton energy spectra. We see that the spectral shape used in MENEKA does not allow for a perfect fit; the deviations for large proton energies carry over to deviations in the $P_{\rm rel}$ spectrum shown in Fig. 13(b). In separate calculations we have shown that such deviations in the spectral shapes have rather little impact on the correlation function since they are carried into both the numerator and the denominator. It is mainly the time delay spectrum that matters. The calculated time delay spectrum that results from the multistep evaporation model is shown in the inset, Fig. 13(d); it gives an initial half-life $t_{1/2} \approx 70$ x 10^{-22} s or mean life of $\tau \approx 100$ x 10^{-22} s. In Fig. 13(c) we see that the model description of the data is not unreasonable. The major point here is that the correlations are weak and the effective mean lifetime is correspondingly rather long.

The calculated correlation functions are quite weak, in agreement with the data. These weak correlations result from an accumulation of time intervals over the randomly selected steps. The average number $\langle N_{\rm step} \rangle$ of evaporated light particles (n, p, d, t, α), predicted for an equilibrated ^{148}Tb (with an average spin $J_{\rm rms} \approx 50\hbar$), is calculated [31] to be $\langle N_{\rm step} \rangle \approx 8.6$. Although the initial mean lifetime is calculated to be close to 1 x 10^{-21} s, it is relatively rare that one selects particles from steps 1 and 2. More often, at least one of the particles is chosen later in the chain, thus giving a much greater average time interval, especially for protons since their emission probability is quite uniform over all the cascade.

For the 680 MeV ^{40}Ar reaction, similar comparisons are shown for ^{1}H-^{1}H pairs in Fig. 14. For this case the calculated anticorrelations are much stronger. The reason for this is clear from the trend of calculated lifetimes; we see in Fig. 6 that the average statistical-model lifetimes are ≤ 5 x 10^{-22} s for each of the first seven emission steps while the latter steps follow rather closely the trend for the 312 MeV reaction. This calculated result is also shown in the difference between the time delay curves obtained for each energy as shown in Figs. 13(d) and 14(d).

In the framework of the statistical model the selection of the rare *d-d* pairs or even more rare *t-t* pairs would bias the probability for emission toward the earlier and hotter emitters. This bias of emission probabilities [33] is shown in Fig. 15 for ^{1}H versus ^{2}H versus ^{3}H; with these input probabilities the statistical-model predictions can be expected to give stronger anticorrelations for ^{2}H-^{2}H and ^{3}H-^{3}H compared to ^{1}H-^{1}H. This arises from the respective relative yields of these hydrogen isotopes; for ^{1}H the emission yield is rather uniformly spread over 14 steps, whereas the ^{2}H yields are heavily weighted toward the first half of the chain where the time delays are short. This bias is even stronger for tritons, since their relative emission probabilities drop even faster after the tenth step of the cascade.

The statistical model predictions for ^{2}H-^{2}H and ^{3}H-^{3}H pairs are shown to be in good agreement with the observed correlation functions. These comparisons are shown in Figs. 16 and 17, respectively, for the ^{2}H-^{2}H and ^{3}H-^{3}H cases. First we see from these figures that the ^{2}H

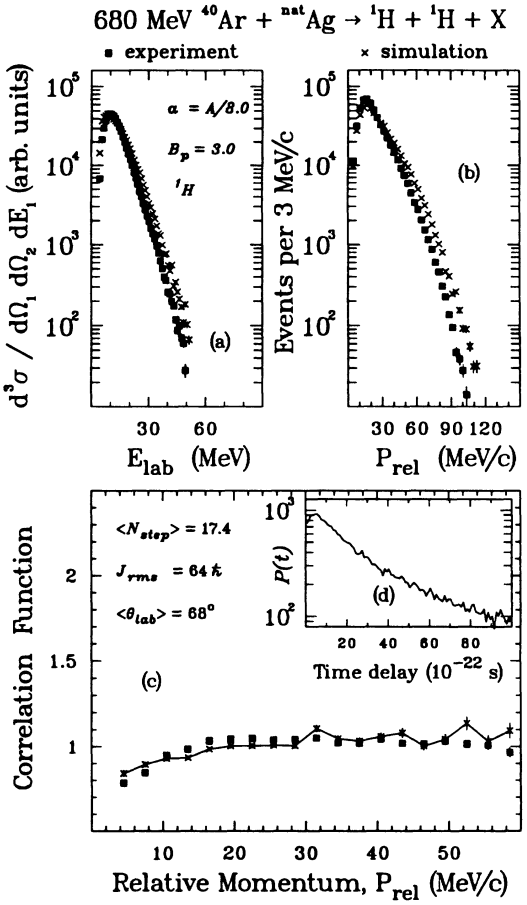

FIG. 14. Experimental and calculated (a) energy spectra, (b) relative momentum, (c) correlation functions, and (d) time delay distribution for ^{1}H-^{1}H pairs at 17A MeV ^{40}Ar + $^{\rm nat}$Ag.

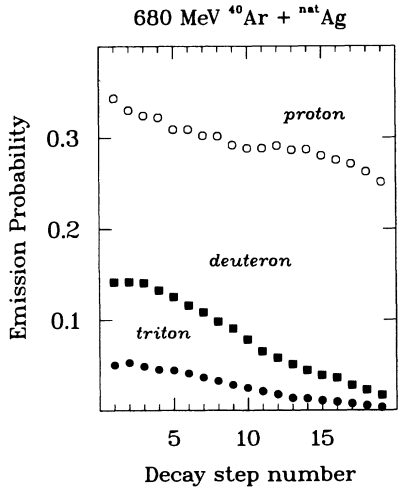

FIG. 15. Statistical predictions for the emission probabilities of ^{1,2,3}H from evaporationlike reactions at 680 MeV ^{40}Ar + $^{\rm nat}$Ag assuming 85% linear momentum transfer (energy mass).

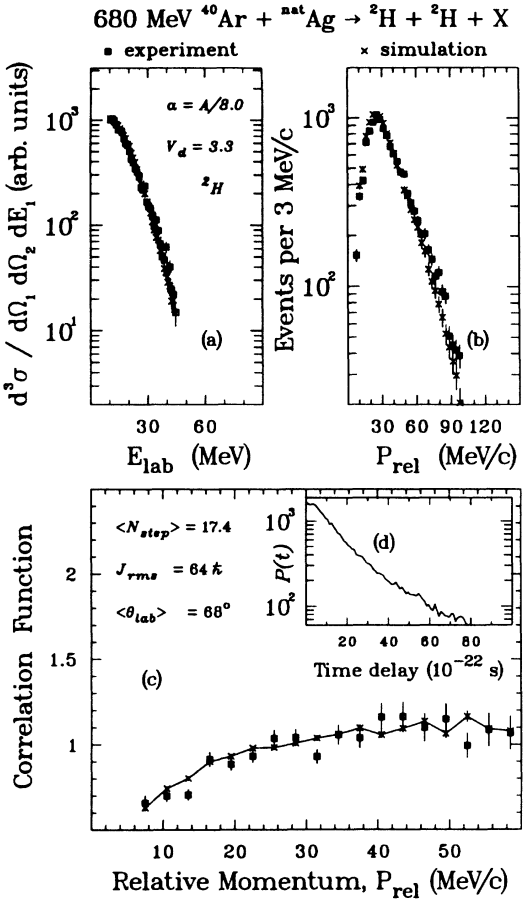

FIG. 16. Experimental and calculated (a) energy spectra, (b) relative momentum, (c) correlation functions, and (d) time delay distribution for ^{2}H-^{2}H pairs at 17A MeV ^{40}Ar + ^{nat}Ag.

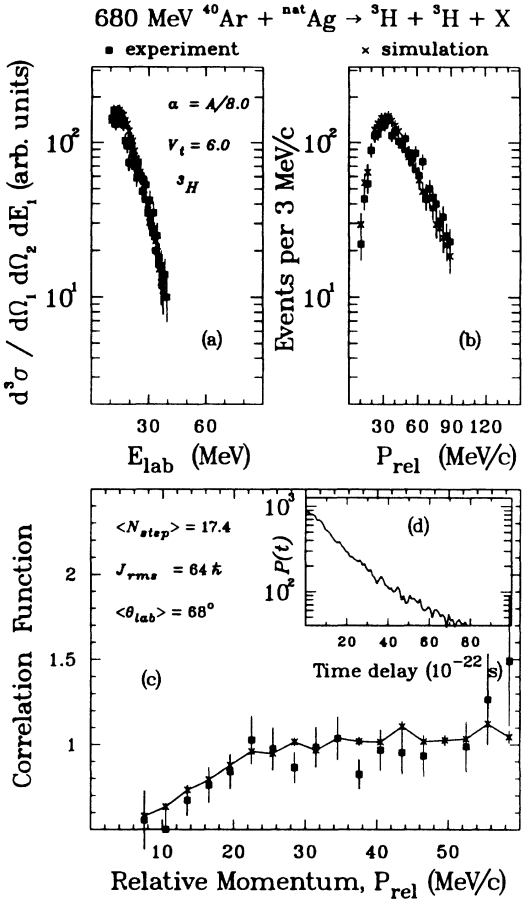

FIG. 17. Experimental and calculated (a) energy spectra, (b) relative momentum, (c) correlation functions, and (d) time delay distribution for ^{3}H-^{3}H pairs at 17A MeV ^{40}Ar + ^{nat}Ag.

and ^{3}H energy spectra are well reproduced with a value for the level density parameter $\mathbf{a} = A/8.0$.

These energy spectra do subsequently lead to a good representation of the associated $P_{\rm rel}$ spectra. Comparison of the correlation functions shown in Figs. 16(c) and 17(c) does indicate that the sequential emission approach seems to be acceptable for these processes. Evidence for average delay time as the major driving force can be based on the slopes of the time distributions shown in Figs. 16(d) and 17(d). The calculated average value for the emission time delays are $\langle t^{dd}_{\rm del}\rangle \approx 20 \times 10^{-22}$ s, and $\langle t^{tt}_{\rm del}\rangle \approx 10 \times 10^{-22}$ s.

These $\langle t_{\rm del}\rangle$ values do agree with the statistical model predictions for the expected decrease in the time scales for the emission of tritons versus deuterons versus protons and thus give support to the model. However, one must point out that the stepwise values of τ as shown in Fig. 6 descend to the incredibly short times of $\approx 10^{-22}$ s for $T \approx 4.2$ MeV. It seems likely that dynamical limits may come into play and override the phase space considerations that give the statistical-model predictions.

V. MULTISTEP EMISSION WITH A DIFFERENT APPROACH TO THE TIME SEQUENCE

In the last section we showed that correlation functions for several particle pairs can be accounted for by sequential particle evaporation. The problem with this approach is the fact that one is ascribing incredibly short mean lifetimes ($\approx 10^{-22}$ s) to the first several steps of the evaporation chain. These calculated lifetimes were derived from a formula based only on the available phase space. No dynamical constraints were imposed relative to intrinsic signal velocities and nuclear dimensions. As a rule of thumb it is often said that the nuclear "traversal time" (radius-velocity) will limit the applicability of such a phase space formulation. For the reaction 680 MeV ^{40}Ar + ^{nat}Ag the traversal time is $\approx 5 \times 10^{-22}$ s which is longer than the calculated evaporation time for the first six emission steps. This then presents us with a dilemma, in spite of the relatively good fit of the data by the model calculation.

As a start on the consideration of possible dynamical

effects, we impose a new parametrization for the emission time sequence. The assumption is that a composite system requires a certain minimum time interval τ_{min} to reset its clock between emission steps. For all steps having calculated mean lifetimes τ_i greater than τ_{min}, no alteration is made in the calculational procedure. However, we make two major changes for all steps calculated to have $\tau_i < \tau_{min}$. First these steps are all assigned mean lifetimes $\tau_i = \tau_{min}$; second the emission times for these steps are all calculated from a common time zero. In other words these emission steps are all said to be taking place concurrently with no summation of times (or reset of the clock to zero).

Figure 18 shows two such calculations for τ_{min} values of 1 x 10^{-20} s and 5 x 10^{-22} s. The value $\tau_{min} = 10^{-20}$ s leads to long delay times and weaker anticorrelations than those observed. However for $\tau_{min} = 5 \times 10^{-22}$ s the decay curve is much steeper and the calculation gives a good fit to the data. The decay curve in Fig. 16(d) is very similar to that of Fig. 18(d) even though the associated calculational rules are very different.

In Fig. 19 one can follow more closely the relationship between the calculated decay curves 19(a) and their associated correlation functions 19(b). It is clear that values of $\tau_{min} \geq 5 \times 10^{-21}$ s do not give strong enough anticorrelations to fit the data. For these large values of τ_{min} the decay curves are much flatter than that for $\tau_{min} = 5 \times 10^{-22}$ s; this latter value does provide a good fit to the data.

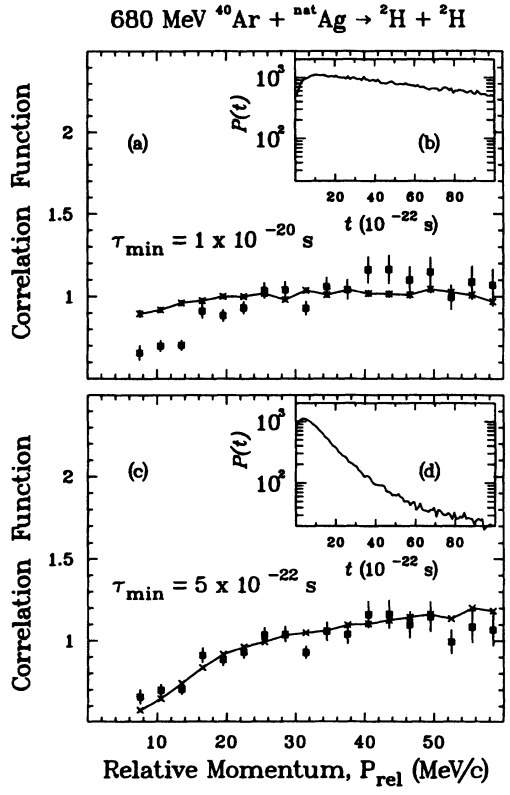

FIG. 18. Correlation function comparisons [(a) and (c)] and time delay distributions [(b) and (d)] for τ_{min} set to 1 x 10^{20} s and 5 x 10^{-22} s for ^{2}H-^{2}H pairs from 17A MeV ^{40}Ar + ^{nat}Ag.

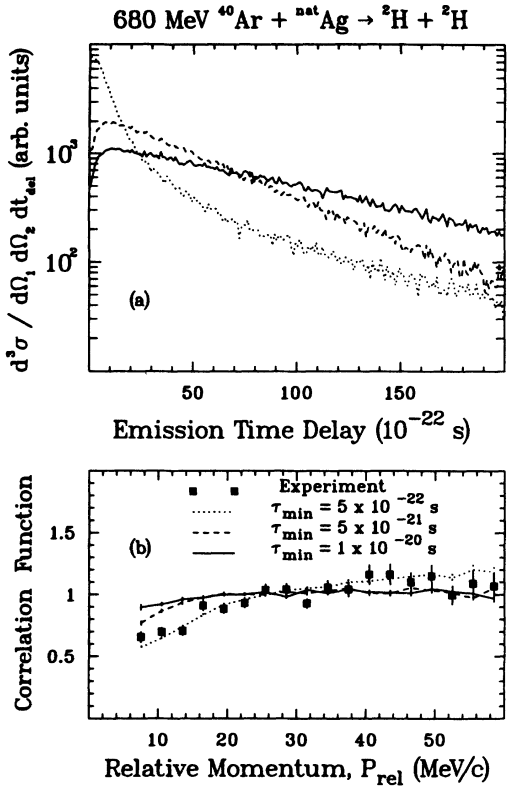

FIG. 19. Time delay distributions (a) and correlation functions comparisons (b) for three τ_{min} values (5 x 10^{-22} s, ◇ and ···; 5 x 10^{-21} s, Δ and - - -; and 10^{-20} s, ○ and —); for ^{2}H-^{2}H pairs from 17A MeV ^{40}Ar + ^{nat}Ag.

A reasonable conclusion is that it is only the decay curve that matters to the calculated correlation functions, not the rules for its formulation. As for the physics of the time scale selection, this comparison seems to suggest that these excited nuclei are at or near the limits for validity of the concept of simple sequential emission. The notion of concurrent evaporationlike emission is therefore suggested. It is interesting that particle and fragment emission times [35] both seem to be $\approx 5 \times 10^{-22}$ s; could this be the dynamical limit for hot composite nuclear decay?

VI. SUMMARY

The main goal of this work has been the study of hot composite nuclear systems first by selecting a reasonably homogeneous set, then by determining their characteristics, and finally by testing their pattern of decay lifetimes.

For ^{40}Ar induced reactions with ^{nat}Ag at two different excitation energies, we characterize the hot composite nuclear emitters via large-angle particle-particle correlations. Evidence is presented for essentially complete energy thermalization, even for composite systems formed at 17A MeV with high initial spin $J_{rms} \approx 64\hbar$ and intial temperature $T \approx 4.5$ MeV.

For these selected emitters we used small-angle particle-particle correlations to probe the decay lifetimes.

These correlation measurements for ^{1}H–^{1}H for both 312 and 680 MeV reactions show consistency with phase space, statistical-model predictions of the evaporation lifetimes. This result implies that evaporative particle emission steps occur with intervals of order 10^{-22} s, a time period comparable to the traversal time for a projectile velocity of 17A MeV. The statistical model predicts even shorter lifetimes as the excitation energy is increased, and indeed we observed stronger correlations for evaporated ^{1}H-^{1}H pairs from composite systems formed in the reaction at 17A MeV compared to 7.8A MeV.

The rare particle pairs, ^{2}H-^{2}H and ^{3}H-^{3}H, were studied for the reaction 17A MeV ^{40}Ar + ^{nat}Ag; these two particle pairs should produce stronger correlations, since they are expected to be preferentially emitted at the earlier steps of the sequential decay cascade. Their small-angle correlations do indeed show stronger correlations compared to the ^{1}H-^{1}H case, and comparisons to multistep emission calculations allow assignment of numerical values for the effective average emission time delays.

ACKNOWLEDGMENTS

Financial support was provided in part by the U.S. Department of Energy and the Centre National de la Recherche Scientifique (France). We are grateful to R. L. McGrath for many helpful discussions.

[1] Conference Proceedings of the Third International Conference on Nucleus-Nucleus Collisions, Saint Malo, France, 1988 [Nucl. Phys. **A488** (1988)].

[2] *Proceedings of the Symposium on Nuclear Dynamics and Nuclear Disassembly*, Dallas, 1989, edited by J. Natowitz (World Scientific Publishers, Singapore, 1989).

[3] *Proceedings of Corinne 90, An International Workshop on Particle Correlations and Interferometry in Nuclear Collisions*, Nantes, France, 1990 (World Scientific Publishers, Singapore, 1990).

[4] S. Kohmoto, M. Ishihara, H. Kamitsubo, T. Nomura, Y. Gono, H. Utsunomiya, T. Sugitate, and K. Ieki, Phys. Lett. **114B**, 107 (1982).

[5] R. Trockel, U. Lynen, J. Pochodzalla, W. Trautmann, N. Brummund, E. Eckert, R. Glasow, K. D. Hildenbrand, K. H. Kampert, W. F. J. Muller, D. Pelte, H. J. Rabe, H. Sann, R. Santo, H. Stelzer, and R. Wada, Phys. Rev. Lett. **59**, 2844 (1987).

[6] P. A. DeYoung, M. S. Gordon, Xiu qin Lu, R. L. McGrath, J. M. Alexander, D. M. de Castro Rizzo, and L. C. Vaz, Phys. Rev. C **39**, 128 (1989).

[7] P. A. DeYoung, C. J. Gelderloos, D. Kortering, J. Sarafa, K. Zienert, M. S. Gordon, B. J. Fineman, G. P. Gilfoyle, X. Lu, R. L. McGrath, D. M. de Castro Rizzo, J. M. Alexander, G. Auger, S. Kox, L. C. Vaz, C. Beck, D. J. Henderson, D. G. Kovar, and M.F. Vineyard, Phys. Rev. C **41**, R1885 (1990).

[8] A. Elmaani, J. M. Alexander, R. Lacey, S. Kox, E. Liatard, F. Merchez, T. Motobayashi, B. Noren, C. Perrin, D. Rebreyend, Tsan Ung Chan, G. Auger, and S. Groult, in *Proceedings of Corinne 90* [3], p. 154.

[9] A. Elmaani, N. N. Ajitanand, J. M. Alexander, R. Lacey, S. Kox, E. Liatard, F. Merchez, T. Motobayashi, B. Noren, C. Perrin, D. Rebreyend, Tsan Ung Chan, G. Auger, and S. Groult, Phys. Rev. C **43**, R2474 (1991).

[10] R. Lacey, N. N. Ajitanand, J. M. Alexander, D. M. de Castro Rizzo, G. F. Peaslee, L. C. Vaz, M. Kaplan, M. Kildir, G. La Rana, D. J. Moses, W. E. Parker, D. Logan, M. S. Zisman, P. DeYoung, and L. Kowalski, Phys. Rev. C **37**, 2540 (1988); **37**, 2561 (1988).

[11] T. Ericson, Adv. Phys. **9**, 423 (1960).

[12] M. Lefort, J. Phys. (Paris) Colloq. **37**, C5-57 (1976).

[13] L. Vaz, J. M. Alexander, and N. Carjan, Z. Phys. A **324**, 331 (1986), and references therein.

[14] J. Galin, in *Proceedings of the International Conference on New Nuclear Physics with Advanced Techniques*, Ierapetra, Greece, 1991 (World Scientific Publishers, Singapore, 1991), p. 131; GANIL report, 1990, p. 90-17.

[15] T. Ethvignot, A. Elmaani, N. N. Ajitanand, J. M. Alexander, E. Bauge, P. Bier, L. Kowalski, M. T. Magda, P. Désequelles, H. Elhage, A. Giorni, D. Heuer, S. Kox, A. Lleres, F. Merchez, C. Morand, D. Rebreyend, P. Stassi, J. B. Viano, S. Benrachi, B. Chambon, B. Cheynis, D. Drain, and C. Pastor, Phys. Rev. C **43**, R2035 (1991).

[16] M. T. Magda, T. Ethvignot, A. Elmaani, J. M. Alexander, P. Désesquelles, H. Elhage, A. Giorni, D. Heuer, S. Kox, F. Merchez, C. Morand, D. Rebreyend, P. Stassi, J. B. Viano, S. Benrachi, B. Chambon, B. Cheynis, D. Drain, and C. Pastor, Phys. Rev. C **45**, 1209 (1992).

[17] B. B. Back, K. L. Wolf, A. C. Mignerey, C. K. Gelbke, T. C. Awes, H. Breuer, V. E. Viola, and P. Dyer, Phys. Rev. C **22**, 1927 (1980).

[18] H. Delagrange, D. Logan, M. F. Rivet, M. Rajagopalan, J. M. Alexander, M. S. Zisman, M. Kaplan, and J. W. Ball, Phys. Rev. Lett. **43**, 1490 (1979).

[19] H. Morgenstern, W. Bohne, K. Grabisch, and D. Kovar, Phys. Lett. **113**B, 463 (1982); H. Morgenstern, W. Bohne, K. Grabisch, H. Lehr, and W. Stoffler, Z. Phys. A **313**, 39 (1983); H. Morgenstern, W. Bohne, W. Galster, K. Grabisch, and A. Kyanowski, Phys. Rev. Lett. **52**, 1104 (1984).

[20] T. Ethvignot, J. M. Alexander, A. J. Cole, A. Elmaani, P. Désequelles, H. Elhage, A. Giorni, D. Heuer, S. Kox, A. Lleres, F. Merchez, C. Morand, D. Rebreyend, P. Stassi, J. B. Viano, F. Benrachi, B. Chambon, B. Cheynis, D. Drain, and C. Pastor, Phys. Rev. C **47**, 2099 (1993).

[21] N. N. Ajitanand, G. LaRana, R. Lacey, D. J. Moses, L. C. Vaz, G. F. Peaslee, D. M. de Castro Rizzo, M. Kaplan, and J. M. Alexander, Phys. Rev. C **34**, 877 (1986).

[22] J. T. Boger, Ph.D. thesis, State University of New York at Stony Brook, 1991.

[23] D. Jacquet, G. F. Peaslee, J. M. Alexander, B. Borderie, E. Duek, J. Galin, D. Gardes, C. Gregoire, H. Fuchs, M. Lefort, M. F. Rivet, and X. Tarrago, Nucl. Phys. **A511**, 195 (1990).

[24] M. F. Rivet, B. Borderie, A. H. Gauvin, D. Gardès, C. Cabot, F. Hanappe, and J. Peter, Phys. Rev. C **34**, 1282 (1986); D. Jouan, B. Borderie, M. F. Rivet, C. Cabot, H. Fuchs, G. Gauvin, C. Grègoire, F. Hanappe, D. Gardès, M. Montoya, B. Remaud, and F. Sèbille, Z. Phys. A **340**, 63 (1991).

[25] D. Drain, A. Giorni, D. Hilscher, C. Ristori, J. Alaria, G. Barbier, R. Bertholet, R. Billery, B. Chambon, B. Chenis, J. Crancon, A. Dauchy, P. Désequelles, A. Fontenille, L. Guyon, D. Heuer, A. Lleres, M. Maurel, E. Monnand, C. Morand, H. Nifenecker, C. Pastor, J. Pouxe, H. Rossner, J. Saint-Martin, F. Schussler, P. Stassi, M. Tournier, and J. B. Viano, Nucl. Instrum. Methods A **281**, 528 (1989).

[26] D. H. Boal, C. K. Gelbke, and B. K. Jennings, Rev. Mod. Phys. **62**, 553 (1990), and references therein.

[27] S. E. Koonin, Phys. Lett. **70B**, 43 (1977).

[28] F. Merchez, S. Kox, C. Perrin, J. Mistretta, J. C. Gondrand, and L. N. Imouk, Nucl. Instrum. Methods **275**, 133 (1989).

[29] N. N. Ajitanand, R. Lacey, G. F. Peaslee, E. Duek, and J. M. Alexander, Nucl. Instrum. Methods Phys. Res. A **243**, 111 (1986).

[30] R. L. McGrath, A. Elmaani, J. M. Alexander, P. A. DeYoung, T. Ethvignot, M. S. Gordon, and E. Renshaw, Comput. Phys. Commun. **59**, 507 (1990).

[31] A. Elmaani, N. N. Ajitanand, T. Ethvignot, and J. M. Alexander, Nucl. Instrum. Methods Phys. Res. A **313**, 401 (1992).

[32] C. J.Gelderloos, J. M. Alexander, J. Boger, P. DeYoung, A. Elmaani, M. T. Magda, A. Narayanan, and J. Sarafa (unpublished).

[33] N. N. Ajitanand and J. M. Alexander, MODGAN, A Modular Nuclear Evaporation Code Based On The Weighted Monte Carlo Technique (to be published). This Hauser Feshbach code continues the approach described in [29,31] with many emitters and multisteps.

[34] A. Elmaaani and J. M. Alexander, Phys. Rev. C **47**, 1321 (1993).

[35] T. Ethvignot, N. N. Ajitanand, C. J. Gelderloos, J. M. Alexander, E. Bauge, A. Elmaani, L. Kowalski, M. Lopez, M. T. Magda, P. Désesquelles, H. Elhage, A. Giorni, D. Heuer, S. Kox, A. Lleres, F. Merchez, C. Morand, D. Rebreyend, P. Stassi, J. B. Viano, F. Benrachi, B. Chambon, B. Cheynis, D. Drain, and C. Pastor, Phys. Rev. C **46**, 637 (1992).